Langmuir

Article

pubs.acs.org/Langmuir

Effect of Contact Line Dynamics on the Thermocapillary Motion of a Droplet on an Inclined Plate

George Karapetsas,*[,†] Kirti Chandra Sahu,[‡] and Omar K. Matar[§]

[†]Department of Mechanical Engineering, University of Thessaly, Volos 38334, Greece

[‡]Department of Chemical Engineering, Indian Institute of Technology Hyderabad, Yeddumailaram 502 205, Andhra Pradesh, India

[§]Department of Chemical Engineering, Imperial College London, London SW7 2AZ, United Kingdom

ABSTRACT: We study the two-dimensional dynamics of a droplet on an inclined, nonisothermal solid substrate. We use lubrication theory to obtain a single evolution equation for the interface, which accounts for gravity, capillarity, and thermocapillarity, brought about by the dependence of the surface tension on temperature. The contact line motion is modeled using a relation that couples the contact line speed to the difference between the dynamic and equilibrium contact angles. The latter are allowed to vary dynamically during the droplet motion through the dependence of the liquid−gas, liquid−solid, and solid−gas surface tensions on the local contact line temperature, thereby altering the local substrate wettability at the two edges of the drop. This is an important feature of our model, which distinguishes it from previous work wherein the contact angle was kept constant. We use finite-elements for the discretization of all spatial derivatives and the implicit Euler method to advance the solution in time. A full parametric study is carried out in order to investigate the interplay between Marangoni stresses, induced by thermo-capillarity, gravity, and contact line dynamics in the presence of local wettability variations. Our results, which are generated for constant substrate temperature gradients, demonstrate that temperature-induced variations of the equilibrium contact angle give rise to complex dynamics. This includes enhanced spreading rates, nonmonotonic dependence of the contact line speed on the applied substrate temperature gradient, as well as "stick−slip" behavior. The mechanisms underlying this dynamics are elucidated herein.

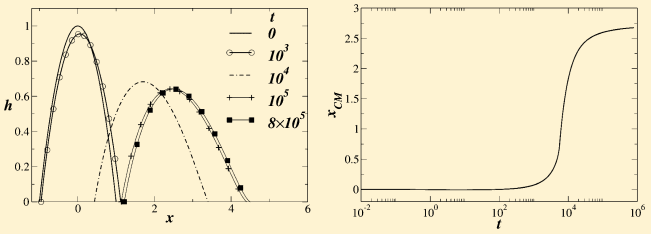

INTRODUCTION

The motion of liquid droplets over liquid and solid substrates has attracted the interest of many researchers in the past because of its numerous practical applications and scientific challenges (see, for example, the reviews by de Gennes[1] and Bonn et al.[2] and references therein). It is well-known that the application of a body force or external gradients can be used as a mechanism for driving the motion of liquid drops, and the ability to control these properties can play a key role in many industrial applications that involve coating processes and microfluidic devices.

In the present work, we focus on the migration of droplets on inclined solid substrates due to the presence of thermocapillary effects. A temperature gradient along the substrate causes another along the interface which may in turn induce surface tension gradients driving liquid flow from warmer to colder regions. Early experimental work by Bouasse[3] has shown that this effect can be used to force a drop to climb a tilted wire, against gravity, by heating its lower end. More recent studies on horizontal plates demonstrated that under certain conditions it was possible to get a steady migration of droplets with a fixed shape; for a temperature gradient below a certain threshold, the drop may not move due to the effect of contact angle hysteresis.[4,5]

It appears, however, that the effect of contact angle hysteresis is not always important. Pratap et al.[6] performed experiments using decane drops on polydimethylsiloxane (PDMS)-coated substrates and showed that the effect of contact angle hysteresis was much weaker. An interesting observation in the experiment of Pratap et al.[6] was the fact that there was a significant dependence of the contact angle on temperature and this was clearly demonstrated by the significant distortion of the footprint of the drop from a circular shape. Pratap et al.[6] have also reported that the experimentally measured migration velocity of the drop was not constant but decreases as the drop moves toward colder regions. They have attributed this effect mainly to the increasing viscosity of the drop and secondarily to the reduction in drop size due to evaporation. However, since in their experiments there was a significant dependence of the contact angle on temperature, it is reasonable to ask whether the variation of the velocity can also be due to the change of wettability as the drop moves to colder regions. One should note that wettability gradients have been proven to be very efficient in driving flow inside liquids.[7,8] Daniel et al.[7] were able to achieve remarkably rapid movement of liquid drops by appropriate manipulation of temperature gradients which altered the wettability of the solid surface. One common factor between the experiments of Pratap et al.[6] and Daniel et al.[7] is

Received: April 20, 2013
Revised: June 11, 2013
Published: June 20, 2013

   dx.doi.org/10.1021/la4014027 | *Langmuir* 2013, 29, 8892−8906

that wettability and temperature gradients coexist. In the present study, the wettability gradients are not imposed externally but are a natural consequence of the variation of temperature along the solid surface.

The thermocapillary motion of droplets has been the subject of several theoretical studies in the literature. Brochard[9] examined the motion of droplets in the presence of chemical or thermal gradients. She assumed that the shape of the drop is a wedge and employed force balance and energy arguments to deduce the wetting characteristics in terms of the spreading coefficient. Ford and Nadim[10] generalized the work of Brochard[9] to allow for arbitrary shapes of the drop and also allowed the contact angles to be different at the two ends. Ehrhard and Davis[11] used lubrication theory to describe the spreading of a droplet on a uniformely heated plate, and Anderson and Davis[12] took into account the effect of evaporation. The latter effect was also studied recently by Karapetsas et al.[13] Chen and co-workers took into account the effect of buoyancy convection[14] and studied the phenomenon of thermocapillary nonwetting.[15]

Lubrication theory was also used by Smith[16] in the presence of thermal gradients to derive quasi-steady solutions employing a dynamic boundary condition at the contact line, which relates the velocity of the contact line to the dynamic contact angle, taking into account the effect of contact angle hysteresis. He showed that only two possible steady states exist: either a motionless drop or a steady migration of the droplet with a fixed shape toward colder regions. Very recently, Gomba and Homsy[17] revisited this problem using lubrication theory in combination with a precursor model to relieve the contact line singularity. The profile of the droplet was allowed to change dynamically with time in the presence of a parametrically varying constant contact angle. They were able to identify three different regimes depending on the contact angles. For small contact angles, the drop spreads with a capillary ridge whereas for large contact angles the drop translates with a fixed shape. For intermediate contact angles, they found a transition regime with rather complex dynamics involving break-up of the drop into smaller droplets.

The results of Gomba and Homsy[17] elucidate the importance of the contact angle in the dynamics of the thermocapillary motion of droplets. The effect of contact line dynamics can be enhanced if we also take into account the effect of the variation of wettability due to the variation of temperature along the solid surface. All of the aforementioned works considered a constant contact angle along the substrate. It is important to investigate what would be the effect of a dynamically varying contact angle which may have a significant impact in cases where there is a strong dependence of the surface energy of the solid substrate on temperature. To the best of our knowledge, this problem has not been addressed in the literature, and this will be one of the aims of this paper. In addition, we will also consider the case of an inclined surface to investigate the interplay of Marangoni stresses, contact line dynamics, and gravity.

The rest of the paper is organized as follows. In section II, we describe the details of the derivation of the evolution equations for the drop profile and temperature, and the numerical method used for their numerical solution. Results are presented and discussed in section III, followed by concluding remarks in section IV.

PROBLEM FORMULATION

We consider the dynamics of a drop of an incompressible, Newtonian fluid with constant density ρ, viscosity μ, specific heat capacity C_p, and thermal conductivity λ, which has been deposited on a inclined, rigid and impermeable solid substrate subjected to a constant temperature gradient (see Figure 1).

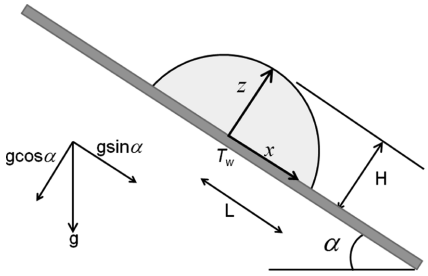

Figure 1. Schematic diagram of the drop on an inclined plate (not to scale). $T_w = T_0 + \gamma x$, where γ is the constant temperature gradient applied at the solid wall and T_0 is the temperature at $(x, z) = (0,0)$.

The angle of inclination to the horizontal is denoted by α. The surface tensions of the liquid−gas, liquid−solid, and solid−gas interfaces are σ_{lg}, σ_{ls}, and σ_{sg}, respectively. We assume that initially the drop has a maximal thickness H and a half-width L. In the present work, we consider the drop to be very thin and therefore L is assumed to greatly exceed H so that the drop aspect ratio, $\varepsilon = H/L$, is assumed to be very small. The latter assumption permits the use of lubrication theory, which will be employed below to derive a set of evolution equations that govern the spreading process.

Governing Equations. We use a Cartesian coordinate system, (x, z), to model the dynamics and the velocity field, $\mathbf{u} = (u,w)$ where u and w correspond to the horizontal and vertical components of the velocity field, respectively. The liquid−gas interface is located at $z = h(x, t)$, whereas the liquid−solid and the solid−gas interfaces are located at $z = 0$. The spreading dynamics are governed by the equations of the conservation of mass, momentum and energy, given below:

$$\nabla\cdot\mathbf{u} = 0 \tag{1}$$

$$\rho(\mathbf{u}_t + \mathbf{u}\cdot\nabla\mathbf{u}) + \nabla p - \mu\nabla^2\mathbf{u} - \rho g = 0 \tag{2}$$

$$\rho C_p(T_t + \mathbf{u}\cdot\nabla T) - \lambda\nabla^2 T = 0 \tag{3}$$

where p is the pressure and T is the temperature, while ∇ denotes the gradient operator. Unless stated otherwise, the subscripts x, z, and t denote partial differentiation with respect to x, z, and t, respectively, where t denotes time.

Solutions of the above equations are obtained subject to the following boundary conditions. Along the free surface, the velocity field should satisfy a local force balance between surface tension and viscous stresses in the liquid, setting the pressure in the surrounding gas to zero (datum pressure) without loss of generality. Taking the tangential and normal to the free surface components of this force balance, we obtain

$$\mathbf{n}\cdot\tau\cdot\mathbf{t} = \mathbf{t}\cdot\nabla_s\sigma_{lg} \tag{4}$$

$$\mathbf{n}\cdot\tau\cdot\mathbf{n} = 2\kappa\sigma_{lg} \tag{5}$$

where $\mathbf{n} = (-h_x,1)/(1 + h_x^2)^{1/2}$ and $\mathbf{t} = (1, h_x)/(1 + h_x^2)^{1/2}$ denote the outward unit normal and unit tangential vectors on

dx.doi.org/10.1021/la4014027 | Langmuir 2013, 29, 8892−8906

the interface, respectively, ∇_s is the surface gradient operator, 2κ is the mean curvature of the free surface, defined as

$$2\kappa = -\nabla_s \cdot \mathbf{n} \tag{6}$$

and

$$\nabla_s = (\mathbf{I} - \mathbf{nn}) \cdot \nabla \tag{7}$$

and τ is the total stress tensor

$$\tau = -p\mathbf{I} + \mu(\nabla \mathbf{u} + \nabla \mathbf{u}^{\mathrm{T}}) \tag{8}$$

where $\mathbf{I}$ is the identity tensor.

In addition, along the moving interface we impose the kinematic boundary condition

$$h_t + uh_x = w \tag{9}$$

and the following thermal flux condition

$$\mathbf{n} \cdot \nabla T = \frac{h_g}{\lambda}(T|_h - T_g) \tag{10}$$

where h_g denotes the heat transfer coefficient at the liquid−gas interface and T_g is the temperature of the ambient gas; for simplification we will assume that $T_g = T_0$, where $T_0 = T(x = 0, z = 0)$.

At the liquid−solid interface, we apply the usual no-penetration condition in the vertical direction

$$w = 0 \tag{11}$$

In the horizontal direction, the usual no-slip condition is replaced by the Navier slip condition[18] to avoid the stress singularity, which would otherwise arise at the moving contact line

$$u = \beta u_z \tag{12}$$

where β is a slip length. We also assume that temperature of the solid surface is fixed and given by the following expression:

$$T_w = T|_0 = T_0 + \gamma x \tag{13}$$

where $\gamma = dT_w/dx$ is the value of the constant temperature gradient applied at the solid wall.

To complete the description, a constitutive equation that describes the dependence of the interfacial tensions on the temperature is required. To this end, we use a simple linear relation

$$\sigma_i = \sigma_{i,0} + \frac{d\sigma_i}{dT}(T_s - T_0), \quad (i = \mathrm{lg, ls, and\ sg}) \tag{14}$$

where T_s is the temperature at the corresponding interface, and $\sigma_{i,o}$, (i = lg, ls, and sg) denotes the surface tension of all interfaces at the reference temperature, T_0.

Scaling. The governing equations and boundary conditions are made dimensionless using the following scalings (tildes denote dimensionless variables)

$$(x, z, h) = L(\tilde{x}, \varepsilon\tilde{z}, \varepsilon\tilde{h}), \quad t = \frac{L}{U}\tilde{t},$$
$$(u, w) = U(\tilde{u}, \varepsilon\tilde{w}),$$
$$p = \frac{\mu UL}{H^2}\tilde{p}, \quad T = \tilde{T}T_0, \quad \sigma_i = \sigma_{\mathrm{lg},0}\tilde{\sigma}_i, \quad (i = \mathrm{lg, ls, sg}) \tag{15}$$

where $U = -(d\sigma_{lg}/dT)(T_0/\mu)$ is a characteristic velocity. The dimensionless numbers that arise are the Bond number $Bo = \rho gH^2/\mu U$, the Biot number $Bi = h_g H/\lambda$, the dimensionless thermal gradient $\Gamma = \gamma L/T_0$, and the dimensionless slip parameter $B = \beta/H$. The tildes are henceforth suppressed.

Substitution of these scalings into the momentum and mass conservation governing equations and boundary conditions, using the lubrication approximation ($\varepsilon \ll 1$), yields

$$u_x + w_z = 0 \tag{16}$$

$$p_x = u_{zz}, \quad p_z = -\varepsilon Bo \cos\alpha \tag{17}$$

$$T_{zz} = 0 \tag{18}$$

$$z = h(x, t)\colon h_t + u|_h h_x = w|_h, \quad p|_h = -\frac{\varepsilon^3 \sigma_{\mathrm{lg}}}{C_{\mathrm{lg}}} h_{xx},$$
$$u_z|_h = \frac{\varepsilon}{C_{\mathrm{lg}}}\sigma_{\mathrm{lg},x}, \quad T_z|_h = -Bi(T|_h - 1) \tag{19}$$

$$z = 0\colon u = Bu_z, \quad w = 0, \quad T_w = 1 + \Gamma x \tag{20}$$

where

$$C_i = -\frac{d\sigma_i}{dT}\frac{T_0}{\sigma_{i,0}}, \quad (i = \mathrm{lg, ls, and\ sg}) \tag{21}$$

It should be noted here that the lubrication approximation assumes small slopes, and therefore this model does not formally capture droplet spreading with high contact angles. By solving eqs 16−18, and imposing boundary conditions 19 and 20 we can derive the following evolution equation for h and temperature T

$$h_t = \frac{\partial}{\partial x}\left[\left(\frac{h^3}{3} + Bh^2\right)p_x - \sigma_{\mathrm{lg},x}\left(Bh + \frac{h^2}{2C_{\mathrm{lg}}}\right) - \frac{h^3}{3}Bo \sin\alpha\right] \tag{22}$$

$$T = T_w\frac{1 + Bi(h - z)}{1 + Bih} \tag{23}$$

where

$$p_x = -\frac{\varepsilon^3}{C_{\mathrm{lg}}}(\sigma_{\mathrm{lg}}h_{xxx} + \sigma_{\mathrm{lg},x}h_{xx}) + \varepsilon Boh_x \cos\alpha \tag{24}$$

and the dimensionless form of the constitutive equation for the surface tension is given by

$$\sigma_{\mathrm{lg}} = \delta_{\mathrm{lg}}(1 - C_{\mathrm{lg}}(T_s - 1)) \tag{25}$$

$$\sigma_i = \delta_i(1 - C_i(T_w - 1)), \quad (i = \mathrm{ls\ and\ sg}) \tag{26}$$

where

$$\delta_i = \frac{\sigma_{i,0}}{\sigma_{\mathrm{lg},0}}, \quad (i = \mathrm{lg, ls, and\ sg}) \tag{27}$$

It follows that the interfacial temperature is $T_s = T|_h = T_w/(1 + Bih)$. For typical experimental conditions, Bi is small ($Bi \ll 1$),[4,5,19] and therefore, for the rest of the paper we will make the assumption that

$$T_s = T_w = 1 + \Gamma x \tag{28}$$

Contact Line Motion. At the contact line, the thickness of the drop becomes zero-valued

dx.doi.org/10.1021/la4014027 | Langmuir 2013, 29, 8892−8906

$$h(x = x_{cl}, t) = h(x = x_{cr}, t) = 0 \tag{29}$$

where x_{cl} and x_{cr} denote the location of the left and right contact lines, respectively. We use an empirical constitutive equation, which relates the fluid velocity at the contact line with the contact angle.[20] In its dimensionless form, ignoring the effect of contact angle hysteresis, to keep the formulation as simple as possible, this relation is given by

$$\frac{dx_{cj}}{dt} = k_j(\theta_j - \theta_{a,j})^m, \quad (j = \text{l and r}) \tag{30}$$

where θ_l and θ_r are the dynamic contact angles at x_{cl} and x_{cr}, respectively, and $\theta_{a,j}$, (j = l and r) are the corresponding advancing contact angles; for the purpose of this study, the latter will be taken to be equal to the equilibrium contact angle, which may vary depending on the temperature of the wall at the position of the corresponding contact line. The model has two empirical constants, the so-called mobility exponents k_j (we will assume that $k_l = k_r = k$), and m which usually takes values in the range $1 \le m \le 3$. This functional dependence has been used by several researchers in the past to model contact line motion.[12,21−25] The power-law dependence has been verified experimentally (e.g., see ref 25). It is worth mentioning that imposing the Navier slip condition away from the contact line and the Cox−Voinov relation at the contact line, mimics the use of the generalized Navier boundary,[26] which relates the contact line speed to a viscous stress contribution (the equivalent of eq 20 in our paper) and an extra contribution due to an uncompensated Young stress (present in out-of-equilibrium situations such as ours). The latter contribution is related directly to the dynamic and static contact angles in a way that is reminiscent of the Cox−Voinov relation, and is much larger (smaller) than the viscous stress contribution at (away from) the contact line. Thus, our approach is rather similar to that involving the use of the generalized Navier boundary condition.

At equilibrium the balance between the tangential interfacial forces at the contact point gives

$$\sigma_{sg}(x_{cj}) = \sigma_{lg}(x_{cj}) \cos \theta_{a,j} + \sigma_{ls}(x_{cj}), \quad (j = \text{l and r}) \tag{31}$$

Using eq 25 in eq 31 and setting $T_s(x_{cj}) = T_w(x_{cj}) = T_{cj}$, ($j$ = l and r), where T_{cj} is the temperature at the contact line, we obtain

$$\cos(\theta_{a,j}) = \frac{\delta_{sg}(1 - C_{sg}(T_{cj} - 1)) - \delta_{ls}(1 - C_{ls}(T_{cj} - 1))}{1 - C_{lg}(T_{cj} - 1)} \tag{32}$$

In the lubrication limit $\theta_{a,j}$ is small. Therefore we set $\theta_{a,j} \to \varepsilon\theta_{a,j}$ and using the fact that $\cos(\varepsilon\theta) = 1 - \varepsilon^2\theta^2/2$, since $\varepsilon \ll 1$, we can then derive the following relation:

$$\theta_{a,j}^{\ 2} = -\frac{2}{\varepsilon^2}\frac{S(1 - C_{sg}\Gamma x_{cj}) - (C_{sg} - C_{lg}) - \delta_{ls}(C_{sg} - C_{ls})\Gamma x_{cj}}{1 - C_{lg}\Gamma x_{cj}} \tag{33}$$

where $S = \delta_{sg} - \delta_{ls} - 1$ denotes the spreading parameter; in order to be consistent with lubrication approximation, S should be kept small. This expression for $\theta_{a,j}$ is used in eq 30 to model the local influence of wall temperature on the contact line velocity. When the right-hand side of eq 33 becomes negative, we simply assume that $\theta_{a,j} = 0$ which implies a perfectly wetting surface. The present method for describing the contact line dynamics can be extended easily to cases where there are wettability gradients of different nature, e.g., involving chemical treatment of the substrate. A similar method has been used previously by Karapetsas et al.[24] to model the effects of surfactants at the contact line in the context of "super-spreading".

In the limiting case where $C_{lg} = C_{sg} = C_{ls}$, the expression for the equilibrium contact angle reduces to

$$\theta_{a,j}^{\ 2} = -\frac{2}{\varepsilon^2}S \tag{34}$$

and therefore the advancing contact angle in this case is independent of the position of the contact line and remains equal to the equilibrium contact angle at the reference temperature. From this, we may deduce that the usual assumption in the literature of a constant equilibrium contact angle simply corresponds to substrates and liquids whose surface tension depends on the temperature in the exact same manner; this is rather restrictive.

Numerical Method. The discretization of the governing equations is performed using a finite element/Galerkin method and we approximate all the variables using quadratic Lagrangian basis functions, ϕ^i. After applying the divergence theorem, the weak form of the governing equations becomes

$$\int_{x_{cl}}^{x_{cr}} (h_t\phi^i + f\phi_x^i)\, dx - [f\phi^i]_{x_{cl}}^{x_{cr}} = 0 \tag{35}$$

$$\int_{x_{cl}}^{x_{cr}} (\bar{h} - h_{xx})\phi^i\, dx = 0 \tag{36}$$

where

$$f = \left(\frac{h^3}{3} + \beta h^2\right)p_x - \sigma_{lg,x}\left(\beta h + \frac{h^2}{2C_{lg}}\right) - \frac{h^3}{3}Bo \sin \alpha \tag{37}$$

and

$$p_x = -\frac{\varepsilon^3}{C_{lg}}(\sigma_{lg}\bar{h}_x + \sigma_{lg,x}\bar{h}) + \varepsilon Boh_x \cos \alpha \tag{38}$$

Note that the fourth order partial differential equation for h has been decomposed into two differential equations by introducing a new variable, $\bar{h} = h_{xx}$.

The initial condition used for the film thickness and the position of the contact line are given by

$$h(x, t = 0) = 1 - x^2 \tag{39}$$

$$x_{cl}(t = 0) = -1 \tag{40}$$

$$x_{cr}(t = 0) = 1 \tag{41}$$

During the spreading process the contact lines move and therefore the physical domain changes with time. In order to map the transient physical domain, (x, t), onto a computational domain fixed in time, (x', t'), we use the following equation:

$$x' = (x - x_{cl})\frac{x_{cr}(t = 0) - x_{cl}(t = 0)}{x_{cr} - x_{cl}} \tag{42}$$

The interior of the drop is mapped to $0 \le x' \le 1$. The derivatives that arise in the evolution equations also have to be rewritten in terms of the new variables

dx.doi.org/10.1021/la4014027 | Langmuir 2013, 29, 8892−8906

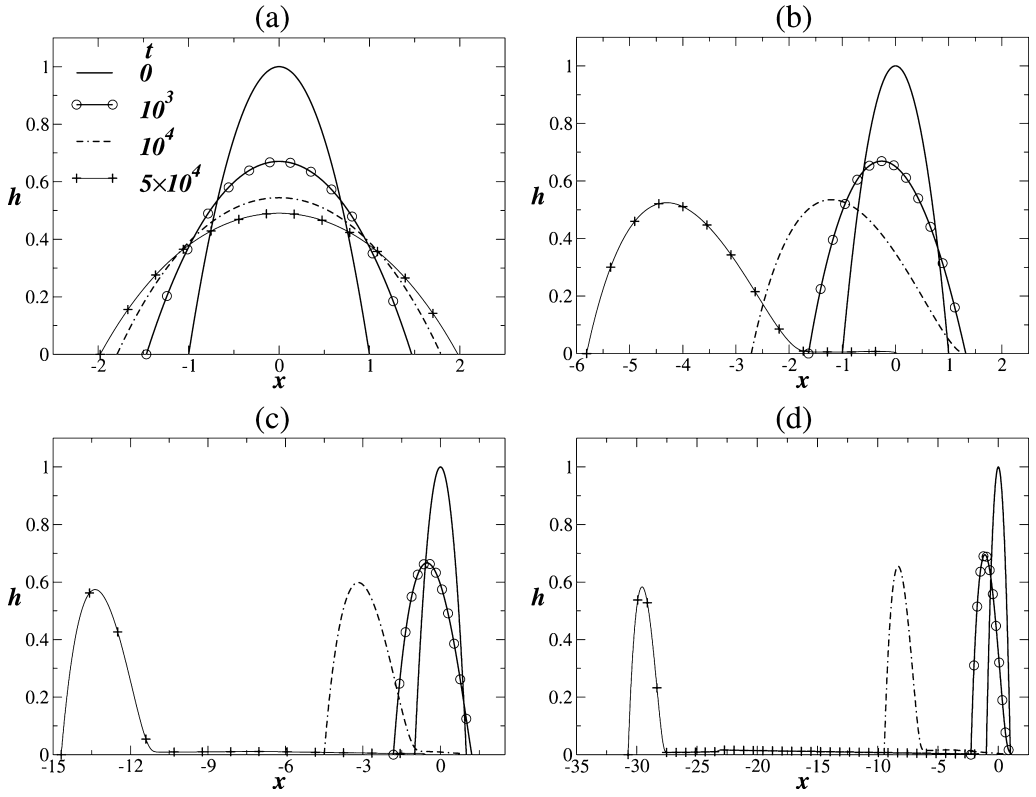

Figure 2. Evolution of the drop profile for (a) $\Gamma = 0$, (b) $\Gamma = 0.005$, (c) $\Gamma = 0.01$, and (c) $\Gamma = 0.02$. The rest of the parameter values are $\varepsilon = 0.1$, $C_{lg} = C_{sg} = C_{ls} = 1$, $k = 10^{-3}$, $m = 3$, $Bo = 0.5$, $\alpha = 0°$, $\delta_{ls} = 1$, and $S = -0.001$.

$$\partial_t = \partial_{t'} - \frac{dx'}{dt}\partial_{x'} \tag{43}$$

and this expression is used to replace the corresponding terms in the weak form of the governing equations presented above.

The computational domain is discretized using 200 elements in all the computations presented in this paper; numerical checks showed that increasing the number of elements further led to negligible changes. In all the simulations presented below the fluid mass conservation are satisfied within 1%. The resulting set of discrete equations is integrated in time with the implicit Euler method. An automatically adjusted time-step is used for that purpose, which ensures convergence and optimizes code performance. The initial time step for all the simulations was 10^{-6}. The final set of algebraic equations is nonlinear and they are solved in each time-step using the Newton−Raphson method. The iterations of the Newton−Raphson method are terminated using 10^{-8} as tolerance for the absolute error of the residual vector.

RESULTS AND DISCUSSION

Numerical solutions were obtained over a wide range of parameter values. For brevity, we choose a representative "base" case that has values $\varepsilon = 0.1$, $k = 10^{-3}$, $m = 3$, $C_{sg} = C_{ls} = 1$, $\delta_{ls} = 1$, and $S = -0.001$. This set of parameters corresponds to slender drops spreading on partially wetting solid surfaces. Considering $C_i \neq 0$ (i = sg and ls) implies that the surface tension of both the solid−gas and liquid−solid interfaces depend on the variation of temperature.

Constant equilibrium contact angle. To set the stage for the discussion that follows, we begin our study by examining the motion of a drop on a horizontal substrate and for the simplest case which predicts a constant equilibrium contact angle. That is true when the surface tension of all interfaces depends in the same way on the temperature, i.e., for $C_{lg} = C_{ls} = C_{sg}$. Using eq 34 we get that for $C_i = 1$, (i = lg, ls, and sg) the equilibrium contact angle remains constant and approximately equal to $\theta_{a,j} = 0.447$, (j = l and r). A typical drop evolution for different thermal wall gradients is presented in Figure 2. As anticipated, we find that for $\Gamma = 0$, i.e., when there is no thermal gradient, the drops spreads symmetrically around $x = 0$ and the radius grows with a power law of $t^{1/7}$ (see Figure 3c), in agreement with its theoretical predictions reported in the literature.[11] On the other hand, as it is shown in Figure 2b−d, the application of a thermal gradient along the wall induces Marangoni stresses which drive the liquid in the drop to flow from hotter to colder regions and thus result in the translation of the drop leaving behind a thin film. The creation of this film is due to the fact that the right edge of the drop spreads initially, but, at the same time, the Marangoni stresses drive liquid flow toward its left edge, thus draining the right edge.

The effect of Marangoni stresses becomes stronger with increasing thermal wall gradient and indeed we see in Figure 3d that the drop translates faster and for longer distances for higher values of Γ. This dependence appears to be monotonic in accordance with earlier studies in the literature.

We observe in Figure 3b that the right contact angle initially advances to the right due to the mismatch of the initial contact angle and the equilibrium contact angle. Eventually, however, the right contact line starts receding due to the effect of the Marangoni stresses which act in the opposite direction. These two mechanisms are also present at the left edge and affect its motion with one important difference. In this case, the mismatch of the initial contact angle with equilibrium contact angle actually enhances the action of Marangoni stresses

dx.doi.org/10.1021/la4014027 | Langmuir 2013, 29, 8892−8906

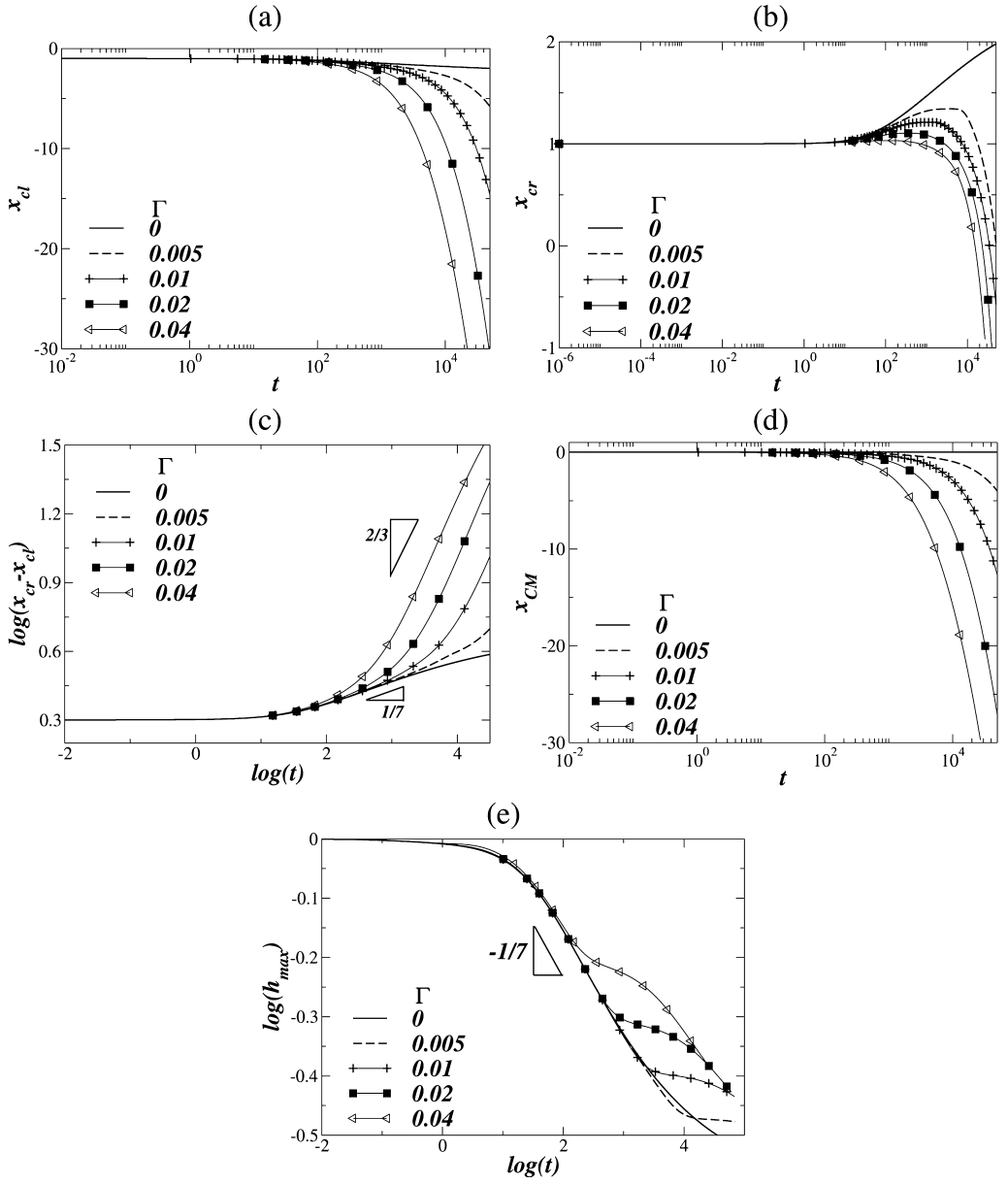

Figure 3. Position of the (a) left and (b) right contact lines of the drop versus time, evolution of the (c) extent of spreading, (d) the position of the center of mass of the droplet, and (e) the maximum height of the drop for different values of Γ. The rest of the parameter values are the same as those used to generate Figure 2.

causing the advancement of the contact line to the left. The combined action of these two mechanisms at the two edges results in enhanced spreading rates and the area covered by the droplet grows with a power-law exponent of order $t^{2/3}$ (see Figure 3c). One should note at this point that the spreading rate predicted by our simulations is significantly larger than the spreading rate predicted earlier by Gomba and Homsy.[17] Gomba and Homsy[17] presented a similarity solution for droplets with small contact angles suggesting that $x_{cr} - x_{cl} \approx t^{1/2}$ and showed that the results obtained from their numerical simulation are in agreement with this scaling law. It should be pointed that in order to derive the similarity solution, Gomba and Homsy[17] ignored the effect of the contact line dynamics. Moreover, their numerical simulations were initiated assuming an equilibrium shape and, therefore, it is expected that, in their case, the contact line dynamics would not play a significant role. On the other hand, we consider drops that are initially far from equilibrium. Indeed, using as initial condition a drop at equilibrium we recover the exponent 1/2, as expected. Therefore, it becomes apparent that the effect of contact line dynamics actually plays an important role leading, in our case, to the prediction of enhanced spreading rates.

Figure 3e shows the evolution of the maximum height of the drop for different values of Γ. At early times, as the drop spreads out its height decreases with $t^{-1/7}$ for all values of Γ. Later on, the drop starts to translate due to the effect of Marangoni stresses which initiates the creation of a trailing film. During this phase, the spreading of the bulk drop ceases and, as a result, the drop height decreases much more slowly. As the drop moves further away from its initial position, the film thickens containing a significant amount of liquid, which leads eventually to the decrease of the drop height.

Varying Equilibrium Contact Angle. As was mentioned above, the assumption of constant equilibrium angle in our

dx.doi.org/10.1021/la4014027 | *Langmuir* 2013, 29, 8892−8906

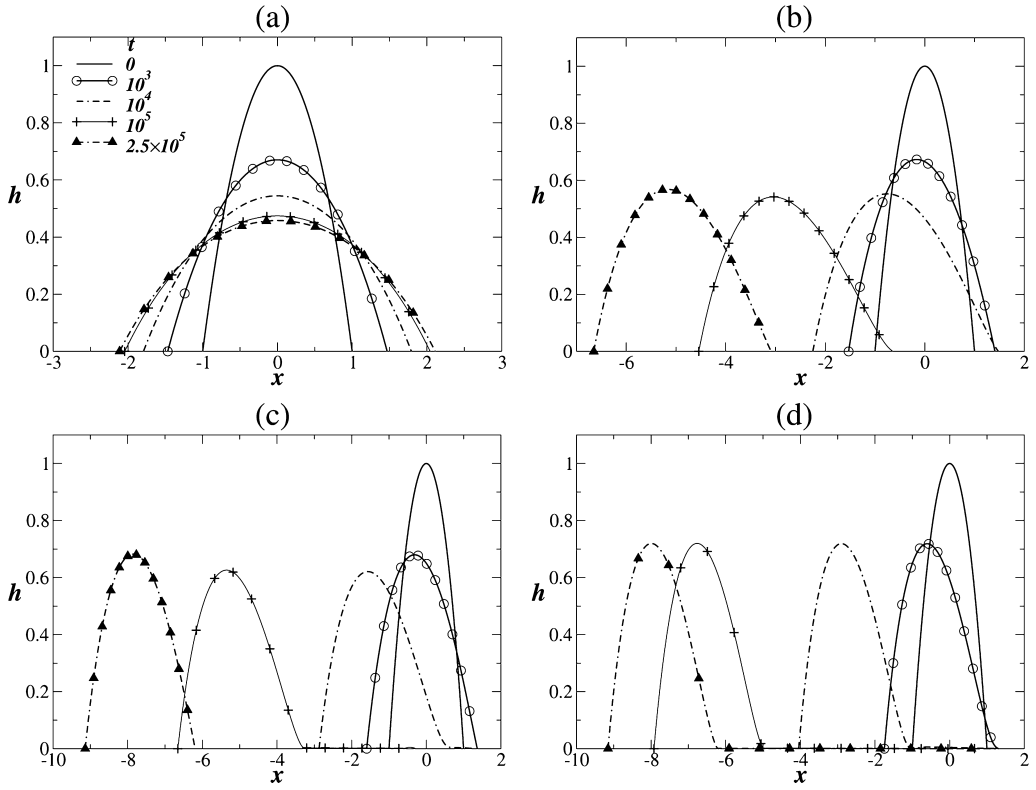

Figure 4. Evolution of the drop profile for C_{ls} = 1.05 and for (a) Γ = 0, (b) Γ = 0.005, (c) Γ = 0.01, and (d) Γ = 0.02. The rest of the parameter values are the same as those used to generate Figure 2.

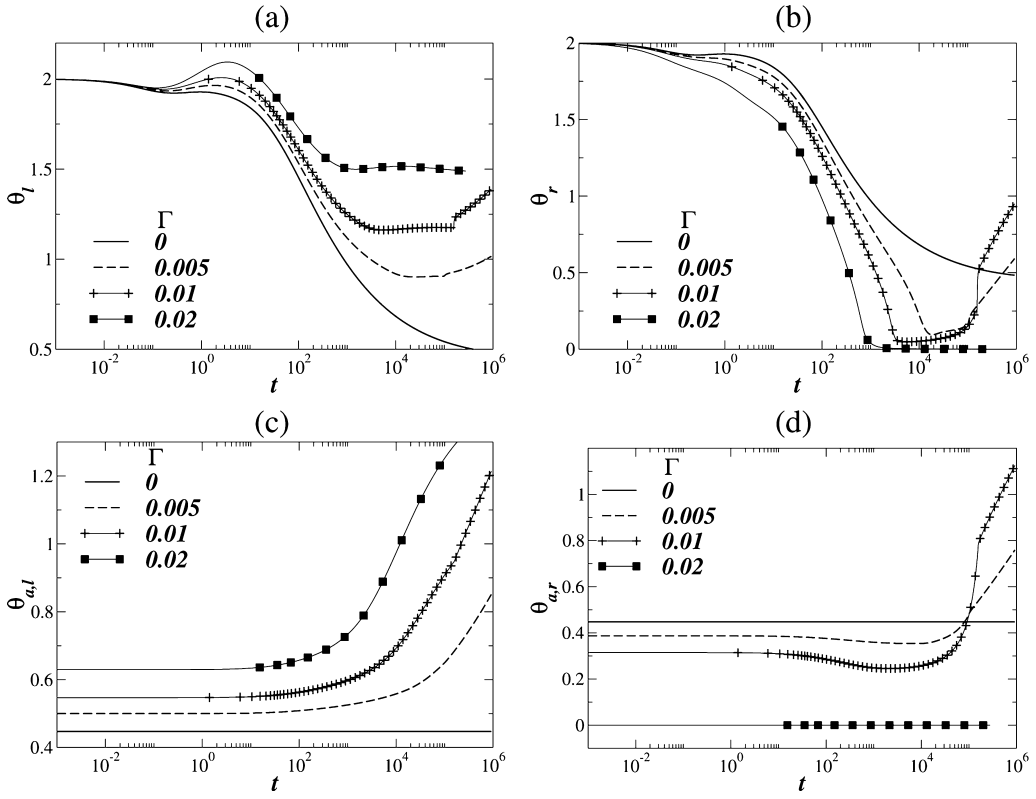

Figure 5. Evolution of dynamic contact angles (a) θ_l and (b) θ_r, and equilibrium contact angles (c) $\theta_{a,l}$ and (d) $\theta_{a,r}$ for different values of Γ. The rest of the parameter values are the same as those used to generate Figure 4.

model corresponds to $C_{lg} = C_{sg} = C_{ls}$. To investigate how deviations from this limiting case may affect the flow, we keep the values of $C_{lg} = C_{sg}$ = 1 and vary slightly the value of C_{ls} = 1.05. The choice of this value of C_{ls} corresponds to a case where

dx.doi.org/10.1021/la4014027 | Langmuir 2013, 29, 8892−8906

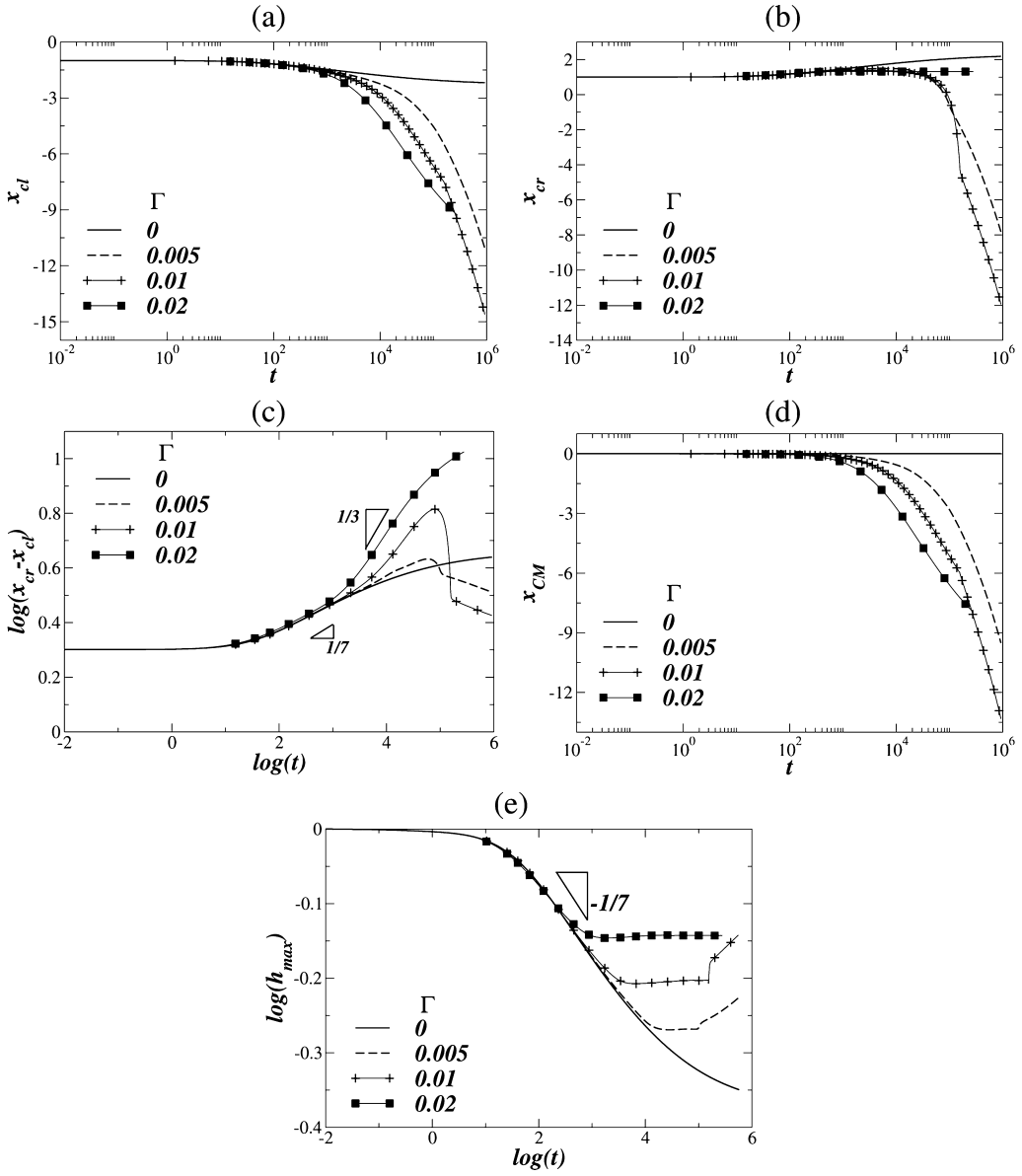

Figure 6. Position of the (a) left and (b) right contact line of the drop versus time, evolution of the (c) extent of spreading, (d) the position of the center of mass of the droplet, and (e) the maximum height of the drop for different values of Γ. The rest of the parameter values are the same as those used to generate Figure 4.

the surface tension of the liquid−solid interface is slightly more sensitive to the variation of temperature as compared to the other two interfaces.

We present in Figure 4 the profiles of the drops at different time instants for different values of Γ. The initial configuration of the drop is such that the dynamic contact angle is larger than the equilibrium contact angle for both edges which causes the initial spreading of the drop in both directions (see Figure 5). In the absence of thermal gradients the drop spreads symmetrically and, as expected, there are no differences between Figures 2a and 4a. On the other hand, for finite values of Γ, the drop spreads initially in both directions, and, at the same time, the induced thermally driven Marangoni stresses drive liquid flow toward colder regions of the substrate. However, as the left edge advances it experiences lower temperatures and as a result the corresponding equilibrium contact angle increases significantly, which implies that the wettability of the substrate changes making it more hydrophobic (see Figure 5c). Consequently, the difference between the dynamic and equilibrium contact angles at the left edge of the drop decreases considerably and the motion of the droplet in that direction decelerates (see Figure 5b,c). As can be deduced from eq 33, the wettability of the substrate is affected most for higher values of Γ, and, for the particular choice of parameters, the left contact line will experience a more hydrophobic substrate closer to the initial position of the drop with increasing Γ.

The change in wettability is also reflected on the migration velocity of the droplet. Comparing the positions of the drop for the two highest values of Γ, we see that at $t = 10^5$ the drop has moved less from its initial position for Γ = 0.01 than for Γ = 0.02 but later catches up. This is shown more clearly in Figure 6a where we have plotted the evolution of the position of the left contact line for various values of Γ. Apparently, for Γ = 0.02 the left contact line decelerates at late times and the drop for Γ = 0.01 appears to be moving faster toward the colder regions of

dx.doi.org/10.1021/la4014027 | Langmuir 2013, 29, 8892−8906

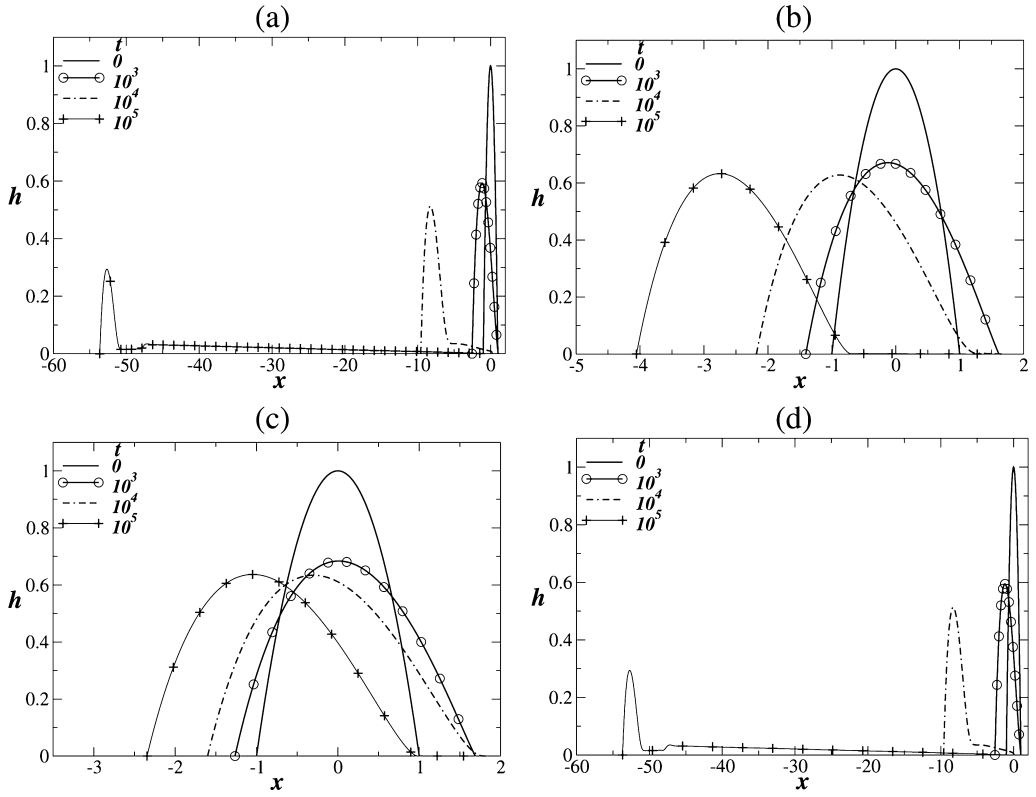

Figure 7. Evolution of the drop profile for (a) $C_{lg} = C_{sg} = 1$ and $C_{ls} = 0.9$, (b) $C_{lg} = C_{sg} = 1$ and $C_{ls} = 1.1$, (c) $C_{lg} = C_{ls} = 1$ and $C_{sg} = 0.9$, and (d) $C_{lg} = C_{ls} = 1$ and $C_{sg} = 1.1$, for $\Gamma = 0.01$. The rest of the parameter values are the same as those used to generate Figure 4.

the substrate (see also Figure 6d where we plot the position of the center of mass of the drop with time). The behavior above is somewhat counterintuitive because we would expect that high thermal gradients would induce high Marangoni stresses which would, in turn, accelerate the motion of the droplet toward lower temperatures of the solid surface. Such behavior has been reported in several theoretical studies in the literature,[10,16,17] and was actually shown to be true in the limiting case of constant equilibrium angles in the previous section. However, the present results clearly show that when we take into account the contact line dynamics and in the general case where the contact angle varies depending on the position of the contact line on the solid surface, the thermocapillary motion of droplets can be significantly more complex.

At this point we should also note that at very late times it is reasonable to expect that the dynamic contact angle at the left edge will eventually become equal to the equilibrium contact angle at which point the motion of the droplet will stop. For the particular set of parameters, it is straightforward to show that the final distance that will be covered by the drop becomes smaller with increasing the wall thermal gradient. Therefore, apart from the nonmonotonic dependence of the translation velocity on the thermal gradient, the inclusion of the contact line dynamics in our model sets a limitation on the motion of the droplet along the substrate in contrast to an infinite motion of the drop under the influence of Marangoni stresses predicted by previous models in the literature.[17] This effect could also provide an explanation for the decrease of the migration velocity observed experimentally by Pratap et al.[6]

On the right edge, we observe that the thin film that follows the drop as it moves toward colder regions in all cases of Figure 2 is no longer present in Figure 4b for $\Gamma = 0.005$. The film appears at early times for $\Gamma = 0.01$ and disappears at later times whereas it seems to persist for very long times for the highest value of $\Gamma = 0.02$ (see Figure 4c,d). For moderate values of Γ, as the drop translates toward colder temperatures, the equilibrium contact angle at the right edge gradually increases and at some point it becomes larger that the dynamic contact angle triggering the retraction of the right contact line which is enhanced by the action of Marangoni stresses. In Figure 6b, we have plotted the evolution of the position of the right contact angle with time which show clearly the retraction of right contact line for intermediate values of Γ. This retraction also results in the significant decrease of the area covered by the drop and that is shown in Figure 6c. For the highest value of $\Gamma = 0.02$, the equilibrium contact angle at the right edge initially happens to be equal to zero (i.e., the contact line feels a hydrophilic substrate from that side) and the liquid wets perfectly the surface from that side. As a result the thin film that is created, in this case, is very stable and remains in place till the end of the simulation.

To explore further the effect of varying substrate wettability due to temperature variation, we impose a constant wall thermal gradient ($\Gamma = 0.01$), and vary the value of C_{ls} and C_{sg}. As shown in Figure 7 even small variations in the value of C_i (i = sg and ls) can have a significant impact on the resulting drop motion by enhancing or inhibiting the translation of the droplet toward colder regions of the wall. These results provide another clear indication that the effect of contact line dynamics should be an integral part of any study of the thermocapillary-driven motion of droplets.

Next we investigate another interesting situation where the interplay between Marangoni stresses and contact line dynamics affect significantly the flow. In Figure 8, we present

dx.doi.org/10.1021/la4014027 | Langmuir 2013, 29, 8892−8906

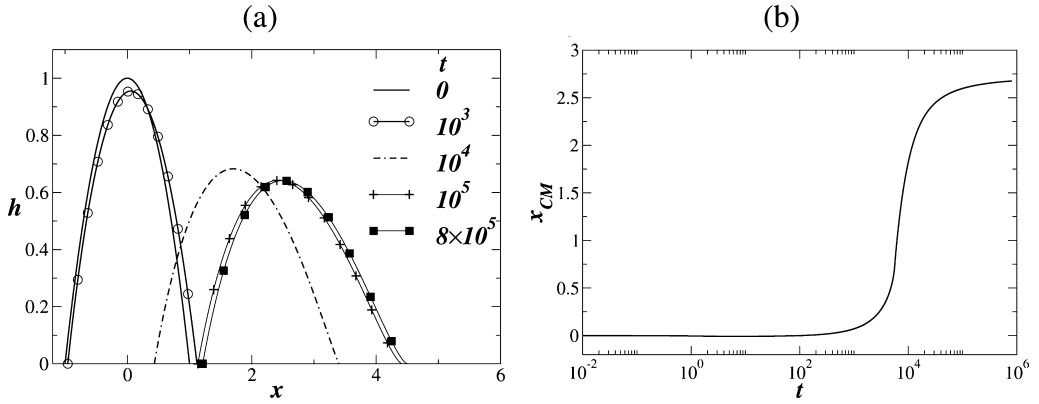

Figure 8. Evolution of the (a) drop profile and (b) position of the center of mass of the drop. The parameter values are $Bo = 0.5$, $\varepsilon = 0.1$, $C_{lg} = 1$, $C_{sg} = 0.5$, $C_{ls} = 1$, $k = 10^{-3}$, $m = 3$, $\Gamma = 0.01$, $\alpha = 0°$, $\delta_{ls} = 1$, and $S = -0.02$.

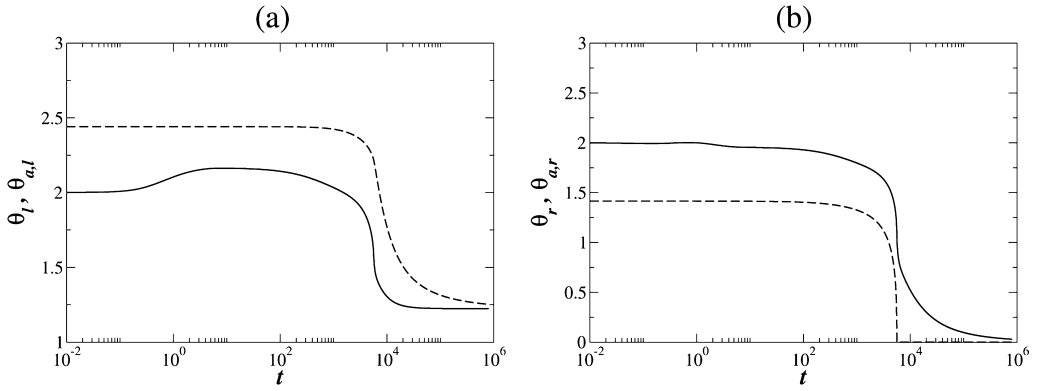

Figure 9. Evolution of (a) left dynamic contact angle, θ_l (solid line) and left equilibrium contact angle $\theta_{a,l}$ (dashed line), and (b) right dynamic contact angle, θ_r (solid line) and right equilibrium contact angle $\theta_{a,r}$ (dashed line) for the parameter values are the same as those used to generate Figure 8.

the case of a droplet that partially wets the solid substrate with spreading parameter $S = -0.02$. In this case, the drop stays stationary for a significant amount of time, then moves rapidly toward the hotter region of the substrate before stopping. This "stick−slip" motion of the droplet is highly unexpected, even more so considering the fact that the drop moves in the opposite direction to the action of Marangoni stresses, which are due to the temperature gradient along the substrate.

To rationalize the above result, we examine the evolution of the dynamic and equilibrium contact angles. In Figure 9, we see that initially, $\theta_l < \theta_{a,l}$ and $\theta_r > \theta_{a,r}$. As a result, if we ignore temporarily the effect of Marangoni stresses, the left and right contact lines will recede and advance, respectively. The action of Marangoni stresses drives fluid flow from right to left, acting to decrease θ_r and increase θ_l. As the right contact line advances, it experiences a hotter substrate and, as a result, the right equilibrium contact angle decreases. The drop experiences an increasingly hydrophilic substrate from that side, and that contact line starts to advance rapidly carrying away the bulk drop. The left contact line moves to the right and experiences higher temperatures which leads to a decrease of the equilibrium contact angle, $\theta_{a,l}$. As soon as the dynamic contact angle becomes equal to the equilibrium contact angle, the motion of that contact line stops. On the right side, the dynamic contact angle continues to decrease as the equilibrium contact angle becomes zero (perfectly wetting substrate); however, Marangoni stresses, which act in the opposite direction, do not allow the bulk drop to be carried away.

It is reasonable to expect that such a "stick−slip" motion will take place for other sets of parameters that will correspond to similar situations as the one described above. More specifically, we expect that such motion would take place when the initial configuration of the drop is such that the contact angles are somewhere in between the corresponding equilibrium contact angles, and the substrate becomes more hydrophilic with the increase of temperature.

Inclined Wall. *Effect of Bo.* Next, we turn our attention to the effect of gravity and to this end we will examine the thermocapillary motion of a droplet along an inclined substrate. Figure 10 presents the evolution of a drop for different values of the Bond number considering an inclination angle, $\alpha = 30°$. Gravity pulls the drop toward the right side whereas the Marangoni stresses act in the opposite direction, since the temperature increases moving to the right ($\Gamma > 0$). We expect that the direction of the motion of the droplet will depend on the magnitude of the Bond number, and the temperature gradient, both of which affect the relative strength of the gravity and Marangoni forces. Indeed it is shown in Figure 10 that for small values of *Bo* the Marangoni stresses dominate causing the translation of the droplet toward the colder regions of the substrate; this is also shown in Figure 11b where we plot the evolution of the position of the center of mass of the droplet. On the other hand, for large values of *Bo* the Marangoni stresses are dominated by gravity, and the drop spreads downslope acquiring a shape that resembles that of a pancake. As shown in Figure 11, the extent of spreading depends

dx.doi.org/10.1021/la4014027 | *Langmuir* 2013, 29, 8892−8906

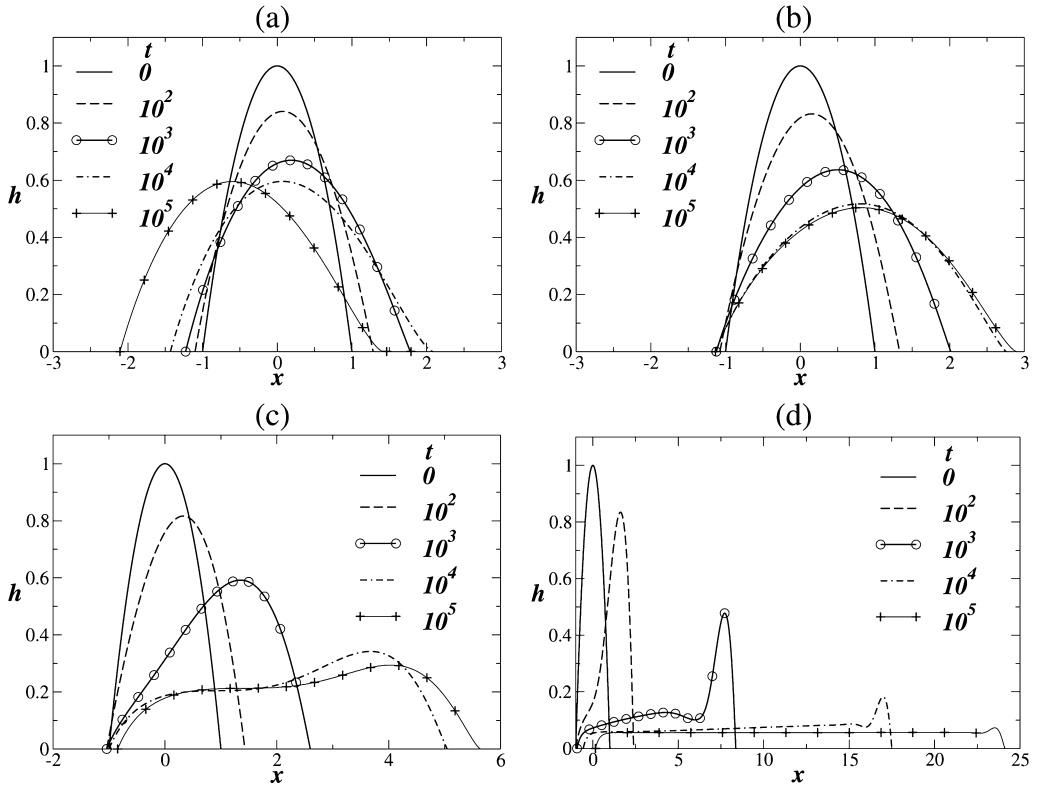

Figure 10. Evolution of the drop profile for (a) $Bo = 0.05$, (b) $Bo = 0.1$, (c) $Bo = 0.2$, and (d) $Bo = 0.8$. The rest of the parameter values are $\varepsilon = 0.1$, $C_{lg} = 1$, $C_{sg} = 1$, $C_{ls} = 1.1$, $k = 10^{-3}$, $m = 3$, $\Gamma = 0.01$, $\alpha = 30°$, $\delta_{ls} = 1$, and $S = -0.001$.

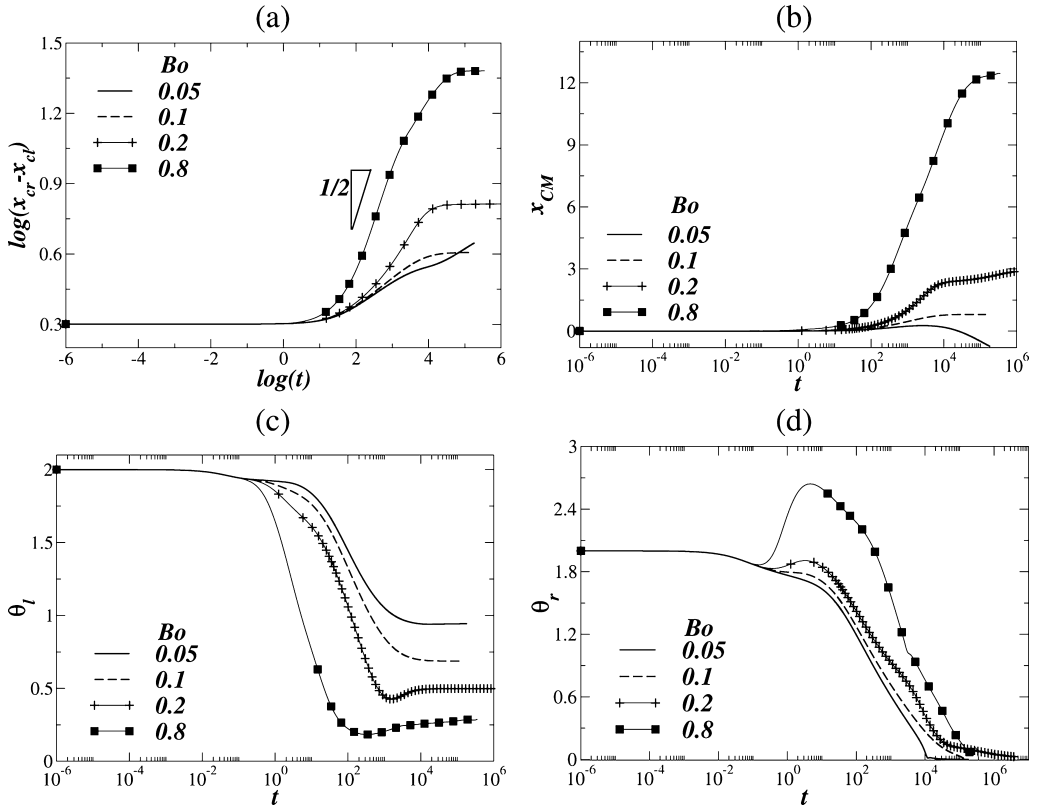

Figure 11. Evolution of the (a) extent of spreading and (b) the position of the center of mass of the droplet and the dynamic contact angles: (c) θ_l and (d) θ_r for different values *Bo*. The rest of the parameters are the same as those used to generate Figure 10.

significantly on *Bo*, and upon comparing with the case of a horizontal substrate, we find that the spreading rate has decreased considerably. This should come as no surprise since in the former case the drop spreading is solely due to the effect

dx.doi.org/10.1021/la4014027 | *Langmuir* 2013, 29, 8892−8906

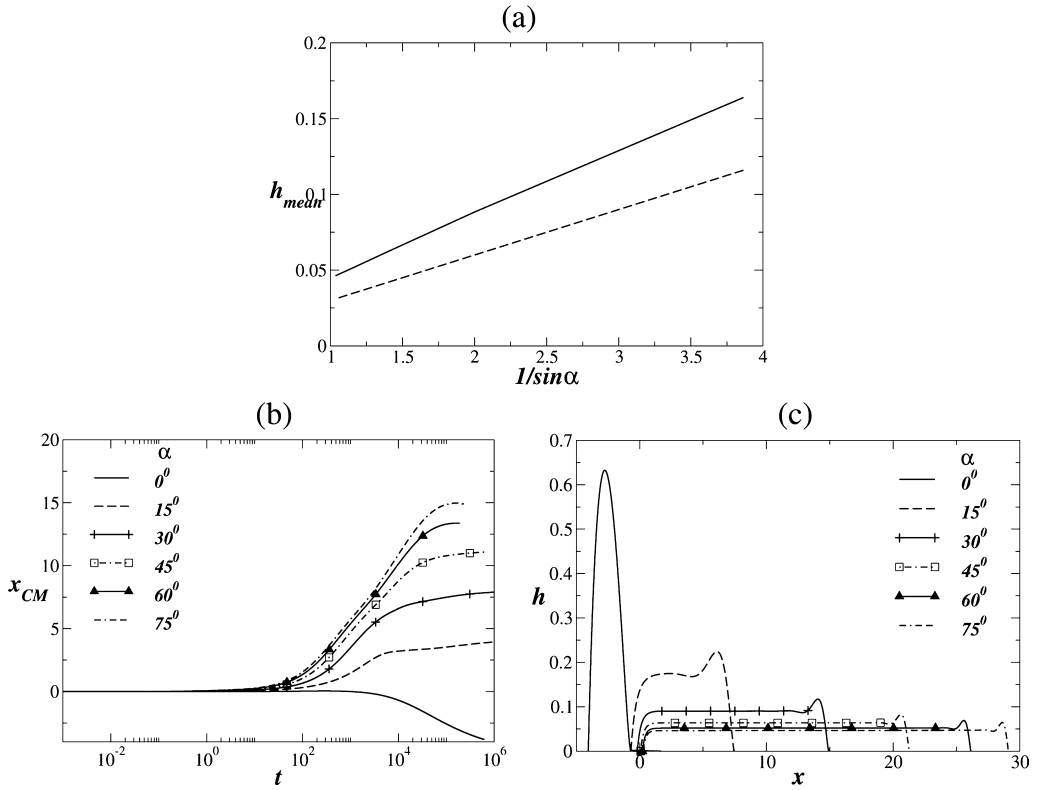

Figure 12. (a) Dependence of the mean height of the droplet, h_{mean}, on the inclination angle; the solid line shows the computed value of h_{mean} at $t = 10^5$ and the dotted line shows h_{mean} as evaluated by eq 44. (b) Evolution of the position of the center of mass of the drop for different angles of inclination and (c) drop profiles at $t = 10^5$. The rest of the parameter values are $\Gamma = 0.01$, $\varepsilon = 0.1$, $C_{lg} = 1$, $C_{sg} = 1$, $C_{ls} = 1.1$, $k = 10^{-3}$, $m = 3$, Bo = 0.5, $\delta_{ls} = 1$, and $S = -0.001$.

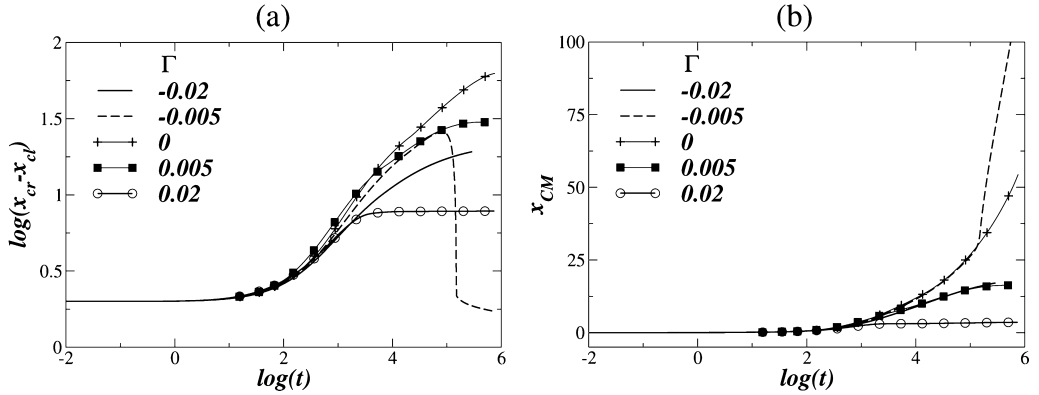

Figure 13. Evolution of (a) the extend of spreading and (b) the position of the center of mass of the droplet for different values Γ. The rest of the parameter values are $\varepsilon = 0.1$, $Bo = 0.5$, $C_{lg} = 1$, $C_{sg} = 1$, $C_{ls} = 1.1$, $k = 10^{-3}$, $m = 3$, $\alpha = 30°$, $\delta_{ls} = 1.0$, and $S = -0.001$.

of Marangoni stresses whereas in the latter case the gravity acts in the opposite direction inhibiting spreading.

As the drop spreads out, its height decreases and this leads eventually to a different balance between Marangoni stresses and gravity. When the action of these two forces becomes equal and the dynamic contact angles approach the equilibrium contact angles, we expect that it would be possible for the drop to reach a steady state. Actually, some of the simulations presented in Figure 11 appear to satisfy these conditions and to have reached such a stationary state. If we ignore the effect of contact line dynamics, it is possible to obtain a rough estimate of the mean height, $h_{mean} = \int_{x_{cl}}^{x_{cr}} h dx / \int_{x_{cl}}^{x_{cr}} dx$ required for gravity and Marangoni stresses to be balanced. Since we seek a steady state solution, we set $h_t = 0$ in eq 22. We also assume curvature and, therefore, the capillary pressure term to be negligible; for negligible slip, we can derive from eq 22 the following expression for the mean height:

$$h_{mean} \approx \frac{3\Gamma}{2Bo} \frac{1}{\sin \alpha} \tag{44}$$

Indeed, when we plot h_{mean} versus $1/\sin\alpha$ in Figure 12a, we find that the slope is approximately equal to $3\Gamma/(2Bo)$, in agreement with eq 44. The small difference in the slope can be attributed to the effect of contact line dynamics, which has been ignored in the analysis above. In Figure 12b, we also present the evolution of the position of the droplet for $Bo = 0.5$ and various angles of inclination; it is shown that for all angles (except for

dx.doi.org/10.1021/la4014027 | Langmuir 2013, 29, 8892−8906

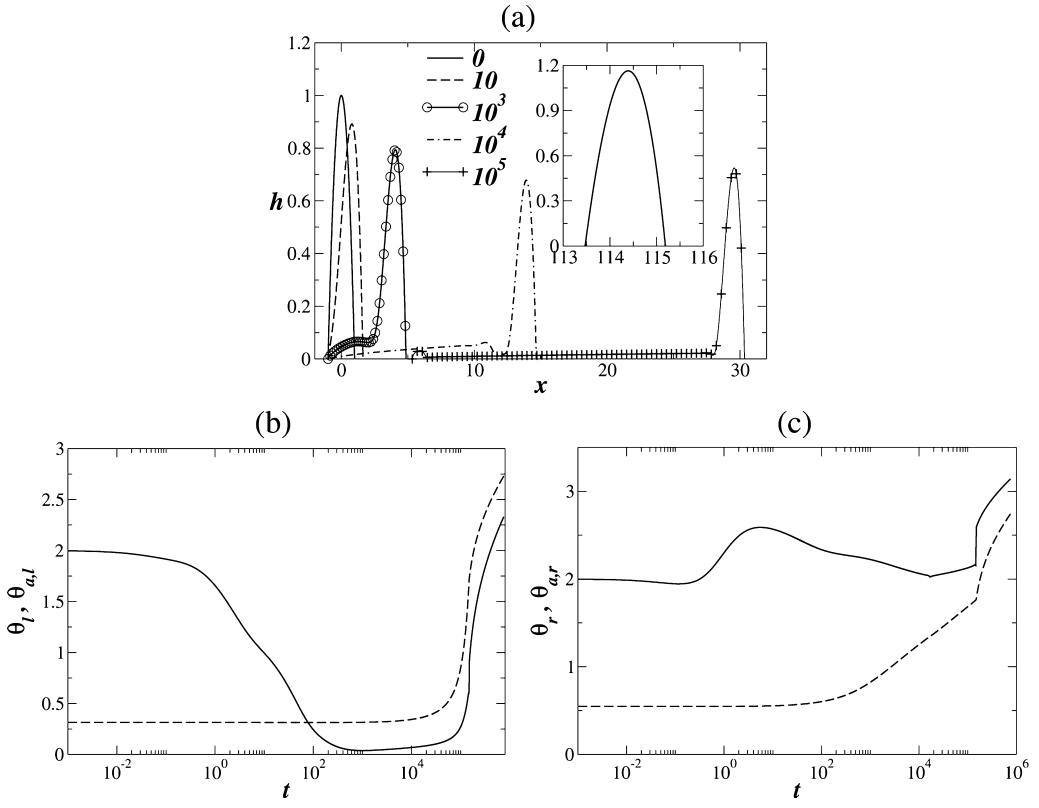

Figure 14. Evolution of the (a) drop profile, (b) left dynamic contact angle θ_l (solid line) and left equilibrium contact angle $\theta_{a,l}$ (dashed line), and (c) right dynamic contact angle θ_r (solid line) and right equilibrium contact angle $\theta_{a,r}$ (dashed line), for $\Gamma = -0.005$. The inset in panel b is the drop profile at $t = 7.5 \times 10^5$. The rest of the parameter values are the same as those used to generate Figure 13.

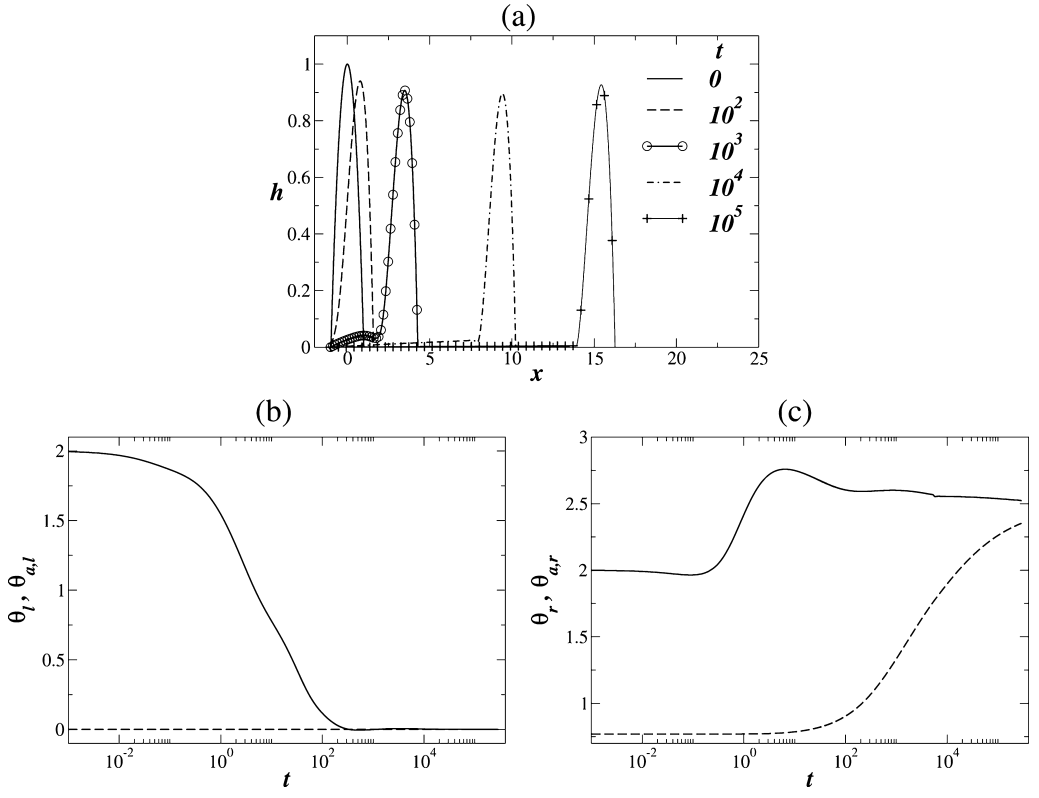

Figure 15. Evolution of the (a) drop profile, (b) left dynamic contact angle θ_l (solid line) and left equilibrium contact angle $\theta_{a,l}$ (dashed line), and (c) right dynamic contact angle θ_r (solid line) and right equilibrium contact angle $\theta_{a,r}$ (dashed line) for $\Gamma = -0.02$. The rest of the parameter values are the same as those used to generate Figure 13.

dx.doi.org/10.1021/la4014027 | *Langmuir* 2013, 29, 8892−8906

the case of a horizontal plate) the motion of the droplet stops as soon as all forces balance. The long-time shapes of the droplet are presented in Figure 12c where we see that for finite values of α the droplet is nearly flat, except for regions near the contact lines where curvature effects are expected to be significant; over the majority of the drop, however, $h \approx h_{mean}$.

Effect of Temperature Gradient, Γ. So far we have examined cases for positive values of Γ, which implies that gravity and the Marangoni stresses act in the opposite direction. We now examine situations where both gravity and Marangoni stresses act in the same direction; this can be achieved by setting $\Gamma < 0$. One may be tempted to assume that, in this case, the droplet will spread less and will move faster downslope because of the combined action of Marangoni and gravity forces. However, as we will see below, the effect of contact line dynamics can be responsible for a much more complex behavior which could not have been predicted easily.

Figure 13a,b presents the evolution of the extent of spreading, and the position of the drop for various values of Γ. For positive Γ, the droplet initially spreads and moves downslope until it reaches a steady state, as described above. For negative values of Γ, on the other hand, the situation varies considerably. We observe in Figure 13b that the migration velocity of the droplet depends in a nonmonotonic way on the magnitude of the temperature gradient. At early times, for $\Gamma = -0.005$ the drop migrates with approximately the same velocity as for $\Gamma = 0$, implying that during this time the action of gravity is dominant. Later on, however, the migration velocity changes drastically and the droplet accelerates significantly for $\Gamma = -0.005$. We also note that during the period of fast motion of the droplet, the extent of spreading decreases abruptly. This happens because the left contact line starts to retract leading to a rapid decrease of the size of the thin film behind the drop until all of it eventually integrates with the bulk drop (see Figure 14a). The retraction of the contact line is triggered when the dynamic contact line becomes smaller than the equilibrium contact line at the left edge as is shown in Figure 14b. When the contact line starts to retract, it comes into contact with a substrate of increasing surface energy due to the effect of temperature. As a result, the retraction of the contact line is accelerated. These results imply that, in this case, Marangoni stresses, gravity forces, as well as the varying substrate wettability, all act cooperatively to enhance the migration of the droplet.

On the other hand, it appears that this is not the case for higher values of Γ, and this can been seen very clearly in Figure 13b. The migration velocity for $\Gamma = -0.02$ is found to be smaller than for $\Gamma = 0$, and the curve that shows the evolution of the position of the center of mass follows closely that for $\Gamma = 0.005$. The evolution of the drop profiles for $\Gamma = -0.02$ is presented in Figure 15 along with the evolution of the dynamic and equilibrium contact angles. We observe that throughout the simulation the film behind the droplet remains stable unlike for $\Gamma = -0.005$. This happens because due to the increased temperature gradient the wettability of the substrate now differs significantly, and the equilibrium contact angle becomes equal to zero, which implies that the solid surface can be fully wetted from the left side stabilizing the film. Therefore, we see that for $\Gamma = -0.02$ the effect of wettability actually inhibits the migration of the droplet, in contrast to what occurs for smaller values of Γ. It becomes apparent that the thermocapillary motion of the droplet is very complex, and the effect of wettability and contact line dynamics should be an integral part of the theoretical study of this problem.

CONCLUSIONS

We have studied the two-dimensional dynamics of a droplet moving on a nonisothermal, inclined solid substrate, heated with constant temperature gradients, bounded from above by a hydrodynamically passive gas. Lubrication theory is used in conjunction with asymptotic reduction to simplify the equations of mass, momentum, and energy conservation, and derive a single evolution equation for the gas−liquid interface. This equation models droplet motion driven by gravity, capillarity, and Marangoni stresses arising from the dependence of surface tension on the local temperature. Crucially, our model also accounts for contact line motion in the presence of dynamically varying substrate wettability brought about by local temperature variations; this, in turn, arises due to local variations of the equilibrium contact angles (at the two edges of the droplet) through their dependence on the temperature-dependent surface tensions of the gas−liquid, liquid−solid, and solid−gas interfaces. This important feature of the model has, to the best of our knowledge, not been taken into account by previous models in the literature in which the contact angles were kept constant; this is valid only when the surface tension of all interfaces has the same dependence on temperature.

We have used a finite-element formulation and an implicit Euler method in time to solve the interface evolution equation. A full parametric study was carried out that focused on the interplay between the effects of the magnitude of the substrate temperature gradient, substrate wettability, Marangoni stresses, and gravity. Results were generated for the spatiotemporal evolution of the droplet shape, and the dynamics of the contact lines, and contact angles for a wide range of parameters starting from drop shapes that are initially far from equilibrium. These results show that for constant equilibrium contact angles, substrate temperature gradients give rise to enhanced spreading rates, characterized by exponents as large as 2/3; these are larger than those predicted by Tanner's law, as as well as the 1/2 exponents obtained for nonisothermal spreading by neglecting the contact line dynamics.[17]

In the presence of temperature-induced wettability variations, the dynamics are rather complex. This is characterized by a nonmonotonic dependence of the droplet center-of-mass velocity on the magnitude of the substrate temperature gradient for horizontal substrates, and situations wherein, for inclined substrates, this monotonicity persists even when the thermal gradient is such that Marangoni stresses are expected to reinforce the action of gravity. We have also found evidence of "stick−slip" contact line motion that arises in cases in which the initial contact angles are between the corresponding temperature-varying equilibrium values. These results show collectively that it is essential to account for variations of the substrate wettability in models of droplet motion over nonisothermal walls.

AUTHOR INFORMATION

Corresponding Author

*E-mail: gkarapetsas@gmail.com.

Notes

The authors declare no competing financial interest.

■ ACKNOWLEDGMENTS

G.K. acknowledges the support by the General Secretariat of Research and Technology of Greece under the action "Supporting Postdoctoral Researchers" (Grant No. PE8/906), cofunded by the European Social Fund and National Resources.

■ REFERENCES

(1) de Gennes, P. G. Wetting: statics and dynamics. *Rev. Mod. Phys.* **1985**, *57*, 827.
(2) Bonn, D.; Eggers, J.; Indekeu, J.; Meunier, J.; Rolley, E. Wetting and spreading. *Rev. Mod. Phys.* **2009**, *81*, 739−805.
(3) Bouasse, H. *Capillarite: phenomenes superficiels*; Librairie Delgrave: Paris, 1924.
(4) Brzoska, J. B.; Brochard-Wyart, F.; Rondelez, F. Motions of droplets on hydrophobic model surfaces induced by thermal gradients. *Langmuir* **1993**, *9*, 2220−2224.
(5) Chen, J. Z.; Troian, S. M.; Darhuber, A. A.; Wagner, S. Effect of contact angle hysteresis on thermocapillary droplet actuation. *J. Appl. Phys.* **2005**, *97*, 014906.
(6) Pratap, V.; Moumen, N.; Subramanian, R. S. Thermocapillary Motion of a Liquid Drop on a Horizontal Solid Surface. *Langmuir* **2008**, *24*, 5185−5193.
(7) Daniel, S.; Chaudhury, M. K.; Chen, J. C. Fast Drop Movements Resulting from the Phase Change on a Gradient Surface. *Science* **2001**, *291*, 633−636.
(8) Wasan, D. T.; Nikolov, A. D.; Brenner, H. Droplets Speeding on Surfaces. *Science* **2001**, *291*, 605−606.
(9) Brochard, F. Motions of droplets on solid surfaces induced by chemical or thermal gradients. *Langmuir* **1989**, *5*, 432−438.
(10) Ford, M. L.; Nadim, A. Thermocapillary migration of an attached drop on a solid surface. *Phys. Fluids* **1994**, *6*, 3183−3185.
(11) Ehrhard, P.; Davis, S. H. Non-isothermal spreading of liquid drops on horizontal plates. *J. Fluid Mech.* **1991**, *229*, 365−388.
(12) Anderson, D. M.; Davis, S. H. The spreading of volatile liquid droplets on heated surfaces. *Phys. Fluids* **1995**, *7*, 248.
(13) Karapetsas, G.; Matar, O. K.; Valluri, P.; Sefiane, K. Convective Rolls and Hydrothermal Waves in Evaporating Sessile Drops. *Langmuir* **2012**, *28*, 11433−11439.
(14) Nguyen, H.-B.; Chen, J.-C. Numerical study of a droplet migration induced by combined thermocapillary-buoyancy convection. *Phys. Fluids* **2010**, *22*, 122101−122101−9.
(15) Chen, J.-C.; Kuo, C.-W.; Neitzel, G. Numerical simulation of thermocapillary nonwetting. *Int. J. Heat Mass Transfer* **2006**, *49*, 4567−4576.
(16) Smith, M. K. Thermocapillary migration of a two-dimensional liquid droplet on a solid surface. *J. Fluid Mech.* **1995**, *294*, 209âĂŞ230.
(17) Gomba, J. M.; Homsy, G. M. Regimes of thermocapillary migration of droplets under partial wetting conditions. *J. Fluid Mech.* **2010**, *647*, 125.
(18) Navier, C. L. M. H. Memoire sur les lois du mouvement des fluides. *Acad. R. Sci. Inst. Fr.* **1823**, *6*, 389−440.
(19) Cazabat, A. M.; Heslot, F.; Troian, S. M.; Carles, P. Fingering instability of thin spreading films driven by temperature gradients. *Nature* **1990**, *346*, 824.
(20) Tanner, L. H. The spreading of silicone oil drops on horizontal surfaces. *J. Phys. D: Appl. Phys.* **1979**, *12*, 1473−84.
(21) Haley, P. J.; Miksis, M. J. The effect of the contact line on droplet spreading. *J. Fluid Mech.* **1991**, *223*, 57−81.
(22) Benintendi, S. W.; Smith, M. K. The spreading of a non-isothermal liquid droplet. *Phys. Fluids* **1999**, *11*, 982−989.
(23) K. Y. Chan, A. B. Surfactant-assisted spreading of a liquid drop on a smooth solid surface. *J. Colloid Interface Sci.* **2005**, *287*, 233−248.
(24) Karapetsas, G.; Craster, R. V.; Matar, O. K. On surfactant-enhanced spreading and superspreading of liquid drops on solid surfaces. *J. Fluid Mech.* **2011**, *670*, 5−37.
(25) Ehrhard, P. Experiments on isothermal and non-isothermal spreading. *J. Fluid Mech.* **1993**, *257*, 463−483.
(26) Qian, T.; Wang, X.-P.; Sheng, P. Molecular scale contact line hydrodynamics of immiscible flows. *Phys. Rev. E* **2003**, *68*, 016306.